Journal of Power Sources 195 (2010) 4104–4113

Contents lists available at ScienceDirect

Journal of Power Sources

journal homepage: www.elsevier.com/locate/jpowsour

Preparation and properties of hybrid direct methanol fuel cell membranes by embedding organophosphorylated titania submicrospheres into a chitosan polymer matrix

Hong Wu[a,b], Weiqiang Hou[a], Jingtao Wang[a], Lulu Xiao[a], Zhongyi Jiang[a,*]

[a] Key Laboratory for Green Chemical Technology, School of Chemical Engineering and Technology, Tianjin University, 92# Weijin Road, Nankai District, Tianjin 300072, China
[b] Tianjin Key Laboratory of Membrane Science and Desalination Technology, Tianjin University, Tianjin 300072, China

ARTICLE INFO

Article history:
Received 20 January 2010
Accepted 27 January 2010
Available online 4 February 2010

Keywords:
Organophosphorylated titania submicrospheres
Hybrid membranes
Direct methanol fuel cell
Methanol permeability
Proton conductivity

ABSTRACT

Organophosphorylated titania submicrospheres (OPTi) are prepared and incorporated into a chitosan (CS) matrix to fabricate hybrid membranes with enhanced methanol resistance and proton conductivity for application in direct methanol fuel cells (DMFC). The pristine monodispersed titania submicrospheres (TiO_2) of controllable particle size are synthesized through a modified sol–gel method and then phosphorylated by amino trimethylene phosphonic acid (ATMP) via chemical adsorption, which is confirmed by XPS, FTIR and TGA. The morphology and thermal property of the hybrid membranes are explored by SEM and TGA. The ionic cross-linking between the $-PO_3H_2$ groups on OPTi and the $-NH_2$ groups on CS lead to better compatibility between the inorganic fillers and the polymer matrix, as well as a decreased fractional free volume (*FFV*), which is verified by positron annihilation lifetime spectroscopy (PALS). The effects of particle size and content on the methanol permeability, proton conductivity, swelling and *FFV* of the membranes are investigated. Compared to pure CS membrane, the hybrid membranes exhibit an increased proton conductivity to an acceptable level of 0.01 S cm^{-1} for DMFC application and a reduced methanol permeability of 5×10^{-7} cm^2 s^{-1} at a 2 M methanol feed.

1. Introduction

Direct methanol fuel cells (DMFC) that use renewable methanol fuel are recognized as an attractive source of power generation, thanks to their high energy density, long lifetime, low pollution, portability and simplified system design [1,2]. However, there exist substantial gaps in current DMFC technology, hindering practical applications. It is possible that these gaps can be bridged with significant improvements in the economical and technical efficiency of DMFC-oriented membranes [3]. State-of-the-art proton-exchange membranes are made of a perfluorosulfonic polymer known as Nafion® (Dupont). The unique structure of this polymer imparts high proton conductivity as well as high mechanical and chemical stability. However, the separated nanophases of hydrophobic and hydrophilic domains cause a serious methanol crossover from the anode to the cathode, reducing the open-circuit potential by as much as 0.15–0.2 V and poisoning the electrocatalysts at the cathode [4]. Additionally, the sharp decline in conductivity above operating temperatures of 100 °C and their high cost considerably limits their applicability [5].

To overcome these limitations, new materials with a controllable structure and superior properties for DMFC are actively being developed [2]. Among them, organic–inorganic hybrid materials have triggered considerable interest due to their extraordinary properties arising from the synergy between the organic moiety and the inorganic moiety. It has been demonstrated that the inorganic fillers within the membrane play an important role in suppressing methanol crossover because they can interfere with polymer chain packing and create a more tortuous diffusion path. Many kinds of inorganic additives, including zeolite [5–7], silica [8,9], montmorillonite [10], zirconium oxide and titanium oxide [11], have been employed to develop hybrid DMFC membranes. In many cases, incorporating these hydrophilic fillers can share the benefit of higher water retention capacity and longer durability of the membranes at elevated temperatures.

However, proton conductivity usually decreases with an increase in filler content due to the rather low proton conductivity of the fillers themselves and their considerable dilution effect on the proton-exchange groups in the original polymer matrix [12]. The direct synthesis and incorporation of proton conductors, such as heteropolyacids (HPA) [13,14] and phosphate particles [15–18] (e.g., zirconium, titanium, silicon and cesium phosphates) is one feasible approach, especially at temperatures above 100 °C. Another approach is achieved by the surface modification of the

* Corresponding author. Tel.: +86 022 23500086; fax: +86 022 23500086.
E-mail address: zhyjiang@tju.edu.cn (Z. Jiang).

0378-7753/$ – see front matter © 2010 Elsevier B.V. All rights reserved.
doi:10.1016/j.jpowsour.2010.01.079

existing fillers via stable acid functionalization [19–25]. Embedding acid-functionalized fillers can potentially enhance or preserve proton conductivity, reduce methanol permeability and optimize the interfacial compatibility of the hybrid membrane.

In this work, a novel type of organophosphorylated titania submicrosphere (OPTi) was synthesized and embedded into a chitosan (CS) matrix to yield hybrid membranes for DMFC. The as-synthesized OPTi particles and the CS–OPTi hybrid membranes were characterized by TEM, FTIR, XPS, SEM and TGA. The effects of OPTi incorporation on membrane properties, including morphology, water uptake, swelling, thermal stability, free volume characteristics, methanol permeability and proton conductivity, were extensively investigated.

2. Experimental

2.1. Materials and chemicals

Chitosan (CS), with a deacetylation degree of 91%, was purchased from Golden-Shell Biochemical Co., Ltd. (Zhejiang, China) and used as received. Amino trimethylene phosphonic acid (ATMP) was supplied by Shandong Taihe Water Treatment Co., Ltd. (Tetrabutyl titanate (TBT), >98%) and ethylene glycol were purchased from Tianjin Guangfu Fine Chemical Research Institute (Tianjin, China). Formic acid, sulfuric acid, acetone, and methanol were of analytical grade and purchased locally. De-ionized water was used throughout the study.

2.2. Preparation of organophosphorylated titania submicrospheres (OPTi)

Titania submicrospheres (TiO_2) of controlled size and low dispersions were synthesized by a modified sol–gel method as described in literature [26]. In a typical synthesis, 0.02 mol TBT was added to 1.28 mol ethylene glycol under nitrogen atmosphere. The precursor solution was magnetically stirred for 10 h at room temperature and then poured into acetone (containing 0.3 wt.% water), with vigorous stirring maintained for 30 min, and then kept undisturbed for 1 h. The final concentration of TBT in acetone varied from 0.01 to 0.07 M. The initially transparent precursor solution became turbid and white, indicating the formation of TiO_2. The white precipitate was separated by centrifugation and rinsed sequentially with water and ethanol to remove excess ethylene glycol. The obtained TiO_2 precipitate was dried overnight at 80 °C. For the phosphorylation of TiO_2, a chemical adsorption procedure, similar to that reported in literature [27,28], was conducted. The TiO_2 powder was first immersed in 25 wt.% ATMP solution under stirring for 12 h at room temperature, and then separated by centrifugation. The powder was rinsed with water repeatedly until the washing solution reached neutral pH, and was then dried at 80 °C for 24 h. The as-synthesized organophosphorylated titania submicrospheres (OPTi) were denoted as OPTi(1), OPTi(3), OPTi(5) and OPTi(7), corresponding to TBT concentrations of 0.01, 0.03, 0.05 and 0.07 M in acetone, respectively.

2.3. Preparation of the CS–OPTi hybrid membranes

The hybrid membranes with different OPTi contents were prepared as follows. Chitosan (1.0 g) was dissolved in 35 mL of 2.0 wt.% aqueous acetic acid solution under constant stirring at 80 °C for 2 h. A desired amount of OPTi was dispersed into 15 mL of 2.0 wt.% aqueous acetic acid solution under ultrasonic treatment for 3 h. Then, the above two solutions were mixed and stirred vigorously at 80 °C for 2 h. After degassing, the resulting homogenous solution was cast onto a clean glass plate and dried at room temperature for 36 h, followed by immersion in 2 M H_2SO_4 solution for 24 h to obtain complete cross-linking. Finally, the membrane was extensively rinsed with water to remove residual H_2SO_4 and dried under vacuum at 25 °C for 24 h. The as-prepared membranes were designated as CS–OPTi(*X*)-*Y*, where *X* (=1, 3, 5 or 7) represented the type of the synthesized OPTi, and *Y* (=5, 10, 15 or 20) was the weight ratio of the filler to CS. Pure CS membrane was also fabricated for the purpose of comparison. The thickness of all of the membranes was within the range of 50–60 μm.

2.4. Characterizations

The morphology of the OPTi submicrospheres was characterized by transmission electron microscopy (TEM, JEOL), whereas the morphology of the membranes was observed using scanning electron microscopy (SEM, Philips XL 30 ESEM), operated at 20 kV. The SEM samples were prepared by freeze-fracturing in liquid nitrogen, and subsequently coated with a thin layer of sputtered gold.

The surface elemental composition of OPTi was characterized by X-ray photoelectron spectroscopy (XPS) using a PHI 1600 spectrometer with Mg Kα radiation for excitation. Fourier transform infrared spectra (FTIR, 4000–400 cm^{-1}) of the fillers and membranes were recorded on a Nicolet MAGNA-IR 560 instrument. Thermo gravimetric analysis (TGA-50 SHIMADZU) data of the fillers and membranes were obtained from 20 to 750 °C using a heating rate of 10 °C min^{-1} under nitrogen flow.

Positron annihilation lifetime spectroscopy (PALS) was performed using a conventional EG&G ORTEC fast–fast coincidence system (resolution 201 ps) at 25 ± 2 °C. The positron source (^{22}Na, 5×10^5 Bq) was sandwiched between two pieces of polymer sample, each with an overall thickness of approximately 1.0 mm. The integral statistics for each spectrum was greater than 2×10^6 coincidences. The spectrum was analyzed using an LT-v9 program.

2.5. Water uptake and area swelling

The water uptake of the membrane was determined by measuring the membrane weight difference before (W_{dry}, g) and after immersion in water for 24 h at room temperature (W_{wet}, g). The area of swelling was determined by comparing the membrane area difference before and after soaking in water. A piece of dry, rectangular-shaped membrane (4.0 cm × 4.0 cm) with an area of A_{dry} (cm^2) was soaked in water for 24 h and then re-measured (A_{wet}, cm^2). The final values of water uptake and swelling were taken as the average of the three measurements with an error within ±3.5% and calculated by Eqs. (1) and (2), respectively:

$$\text{water uptake}\,(\%) = \frac{W_{wet} - W_{dry}}{W_{dry}} \times 100\%, \quad (1)$$

$$\text{area swelling degree}\ (\%) = \frac{A_{wet} - A_{dry}}{A_{dry}} \times 100\%. \quad (2)$$

2.6. Ion-exchange capacity (IEC)

The IEC value of the membrane was measured using a conventional back-titration method. The membrane in H^+ form was immersed in a 2 M NaCl solution for 24 h to completely replace H^+ with Na^+. The remaining solution was then titrated with a 0.01 M NaOH solution using phenolphthalein as an indicator. The IEC value was calculated by Eq. (3),

$$\text{IEC}\,(\text{mmol g}^{-1}) = \frac{0.01 \times 1000 \times V_{\text{NaOH}}}{W_d} \quad (3)$$

where V_{NaOH} (L) is the volume of NaOH solution consumed for titration and W_d (g) is the weight of the dry membrane sample. The measurements were carried out with an accuracy of 0.001 mmol g^{-1}.

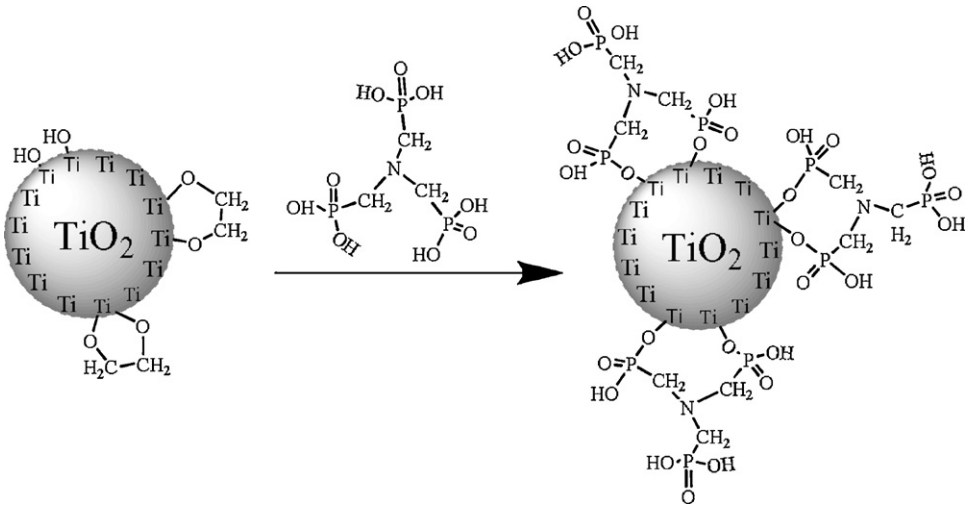

Scheme 1. Organophosphoric acid functionalization of titania submicrospheres.

2.7. Methanol permeability

The methanol permeability was measured with a glass diffusion cell as described in Ref. [20], which consisted of two compartments of identical volume separated by the membrane sheet. The membrane was hydrated in water for 24 h before being clamped tightly between the two compartments. The two compartments were then filled with water and methanol solution (2 or 12 M), respectively. A gas chromatography (Agilent 6820) equipped with a Thermal Conductivity Detector (TCD) and a DB624 column was employed to detect the change in the methanol concentration in the water compartment. The methanol permeability (P, $cm^2\ s^{-1}$) was calculated from Eq. (4),

$$P = S\frac{V_B l}{AC_{A0}} \quad (4)$$

where S is the slope of the straight line of concentration versus time, V_B is the volume of the receipt compartment, and l, A, and C_{A0} are the membrane thickness, effective membrane area and feed concentration, respectively. The measurement errors were all within ±4.0%.

2.8. Proton conductivity

The proton conductivity (σ, $S\,cm^{-1}$) of the membrane in the transverse direction was measured by the AC impedance spectroscopy method at 25 ± 1 °C using a two-point-probe conductivity cell connected to a frequency response analyzer (FRA, Compactstat, IVIUM Tech.) [20]. The measurement was performed in a frequency range of 1–10^6 Hz with an oscillating voltage of 20 mV. All of the membrane samples were immersed in 0.2 M H_2SO_4 for 24 h prior to

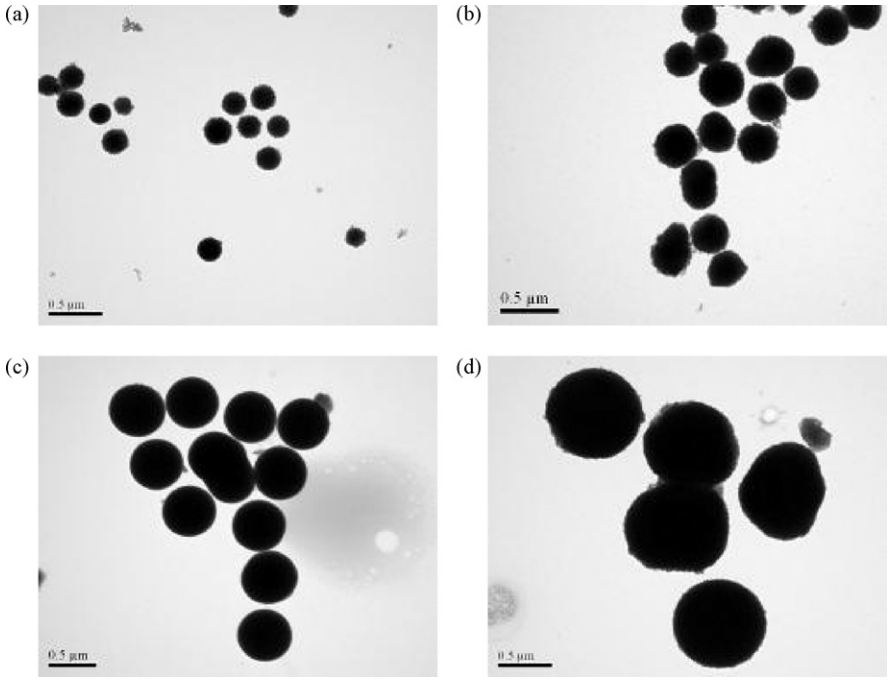

Fig. 1. TEM images of OPTi submicrospheres: OPTi(1) (a), OPTi(3) (b), OPTi(5) (c) and OPTi(7) (d).

measurement. Three measurements were conducted and averaged for each sample with an error within ±5.5% using the equation,

$$\sigma = \frac{1}{AR} \quad (5)$$

where l and A are the thickness and test area of the membrane, respectively, and R is the membrane resistance derived from the low intersection of the high frequency semicircle on a complex impedance plane with Re (z) axis.

3. Results and discussion

3.1. Synthesis and characterizations of OPTi submicrospheres

Titania with high hygroscopicity and thermal stability has been demonstrated as an appropriate fillers for developing hybrid proton-exchange membranes. Among the various sizes of the titania particles embedded in polymer matrices (e.g., nanoparticle [29], nanotube [30] or in situ sol–gel generated [31]), submicron-sized spherical-shaped titania fillers have, to our best knowledge, not been used as additives for hybrid membrane fabrication. To improve proton conductivity and interfacial compatibility of the hybrid membrane, in this study the synthesized titania submicrospheres were further phosphorylated by an organophosphoric acid. Compared to sulfonic acid, the phosphonic acid possesses a lower average zero point energy (37.2 kJ mol^{-1} for phosphonic acid and 69.9 kJ mol^{-1} for sulfonic acid), indicating that the energy penalty in proton transferring from 'acid to acid' via phosphonic acid groups is much less than that via sulfonic acid groups. Moreover, the water binding energy of phosphonic acid (47.3 kJ mol^{-1}) is higher than that of sulfonic acid (44.4 kJ mol^{-1}), suggesting a better water-retaining capacity of phosphonic acid groups under low-humidity conditions [32]. Therefore, phosphorylation of polymers and inorganic fillers by inorganic phosphoric acid has become a promising way to enhance proton conductivity of membranes under intermediate temperature and low relative humidity or even anhydrous conditions [22,23,33–36]. In this study, an organophosphoric acid was utilized in the phosphorylation of titania submicrospheres.

The pristine titania submicrospheres were synthesized by a modified sol–gel process, and the particle size could be conveniently adjusted by varying the TBT precursor concentration. Organophosphorylated titania submicrospheres were then synthesized via the chemical adsorption of organophosphoric acids on the pristine titania particles. Because each ATMP molecule contains three phosphonic acid groups (–PO_3H_2), they could easily form Ti–O–P covalent bonds with the hydroxyl groups (–OH) on the titania surface. As illustrated in Scheme 1, the ATMP ligands were bound to titania in a dentate fashion, generating certain amount of acid sites on the titania surface. The morphology, chemical structure and surface chemistry were probed by TEM, FTIR and XPS.

Fig. 1 shows the morphology of the titania submicrospheres with four different sizes, as observed by TEM. It can be clearly observed that morphologically identical and monodispersed titania submicrospheres with an average particle size of 250, 375, 600 and 875 nm were successfully prepared by simply switching the precursor concentration from 0.01 to 0.07 M.

The chemical structure of OPTi was determined by FTIR. As shown in Fig. 2(a), the absorption bands at 1086, 2868 and 2935 cm^{-1} for pristine TiO_2 were assigned to the C–C–O stretching vibration, symmetric and asymmetric –CH_2– stretching vibrations of ethylene glycol, respectively. The bands around 1400 cm^{-1} were diagnostic of ethylene glycolate ligands in gauche conformation. The bands around 3400 cm^{-1} (the broader band) and 1640 cm^{-1} correspond to the stretching and deformation of adsorbed water molecules and hydroxyl groups on the surface, respectfully. As described in the literature [26], the as-prepared titania submicrospheres were actually titanium glycolate. Herein, the intensity of the band at 570 cm^{-1}, which was assigned to the Ti–O–Ti stretching vibration, was much stronger than that reported in the literature [26,37]. It could be deduced that the titania synthesized in this study was of the Ti–O–Ti structure, and the ethylene glycol was anchored onto the titania surface by forming a bidentate chelate structure between glycol and Ti atoms. This structure would be further confirmed by XPS analysis. After phosphorylation, the characteristic peaks of ethylene glycol at 1086, 1400, 2868 and 2935 cm^{-1} disappeared, and the characteristic peaks of ATMP

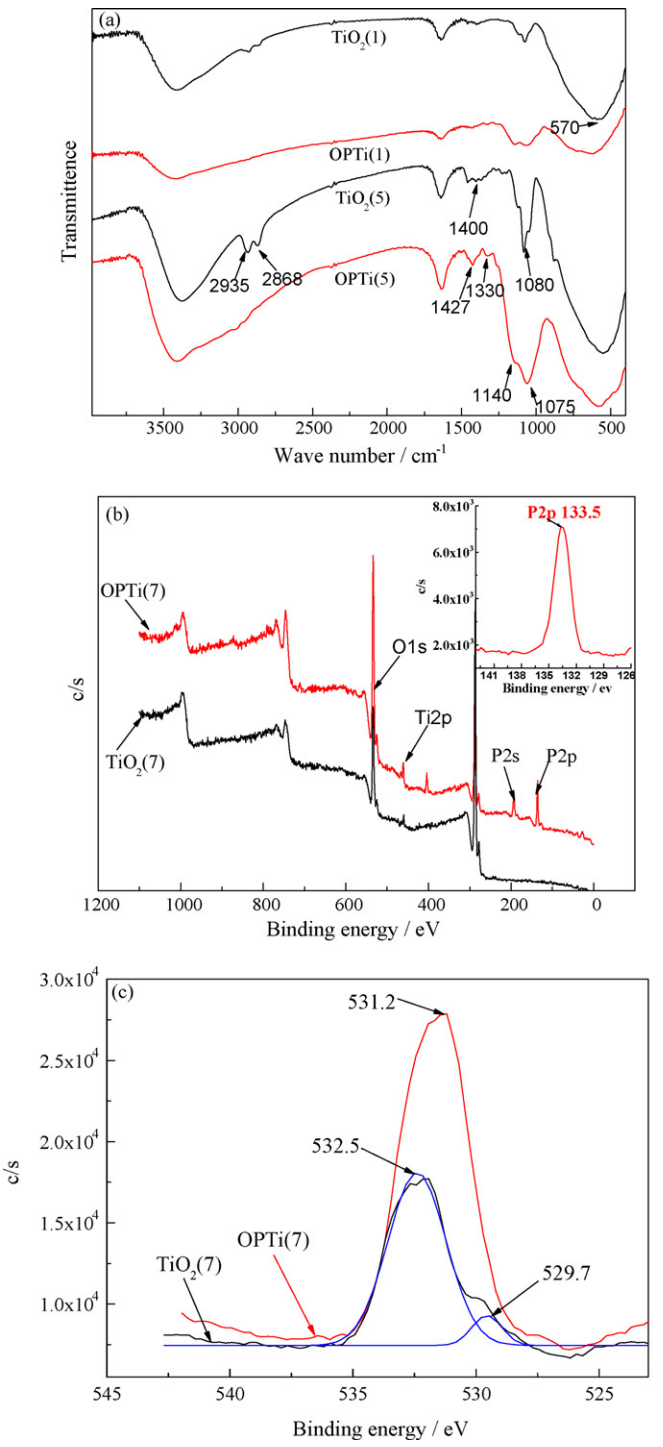

Fig. 2. FTIR spectra (a) and XPS spectra of P 2p and O 1s (b and c) of OPTi submicrospheres.

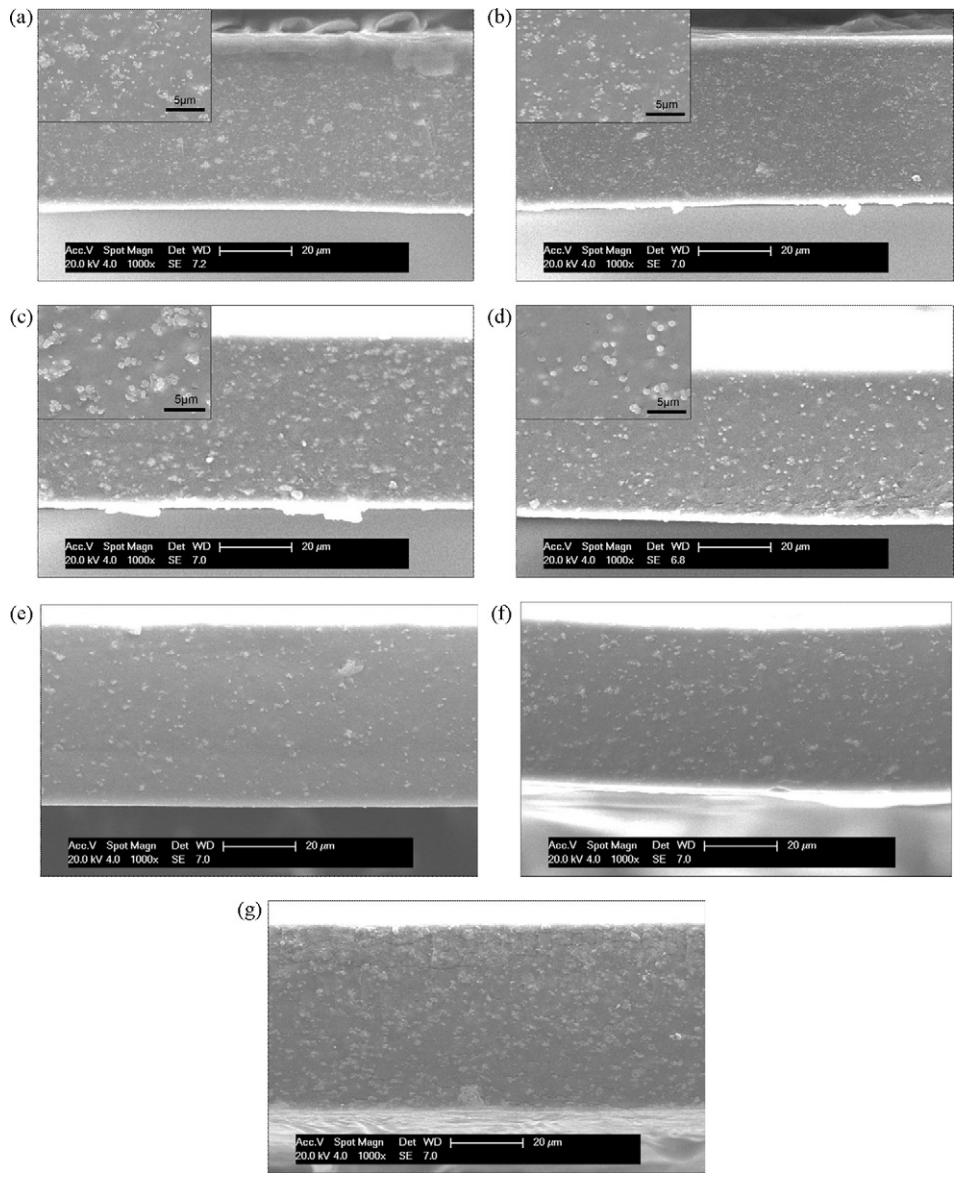

Fig. 3. FESEM images of the cross-sections of CS and CS–OPTi hybrid membranes.

appeared. The new sharp bands at 1075 and 1140 cm^{-1} can be attributed to the P–O–Ti and P═O stretching vibrations, respectively. The bands at 1330 and 1427 cm^{-1} can be attributed to the weak phosphoryl (P═O) frequency and P–C stretching vibrations, respectively [38]. It could be deduced from these results that ATMP had replaced the original chelate position of glycol and formed chemical bonds with the Ti atom at the titania surface via phosphonate groups. To determine the ATMP content on OPTi, TG analysis was performed (data not shown). A weight loss of approximately 12–14% (100–500 °C) was attributed to the decomposition of ATMP that was chemically bound to titanium. The final residue of titania was found to be 81–83%.

XPS was used to further analyze the chemical status of the OPTi(7) submicrospheres. As shown in Fig. 2(b), the main Ti 2p3/2 components of the Ti 2p doublets at 458.7 eV correspond to the O–Ti–O type chemical environment. The binding energy for P 2p of 133.5 eV suggested a pentavalent-oxidation state (P^{5+}) of the phosphorus in OPTi and the presence of the P–O bond. For pristine TiO_2 before organophosphorylation, the O 1s spectrum consisted of two peaks, further deconvoluted and shown in Fig. 2(c); the stronger peak at 532.5 eV can be attributed to the oxygen in the C–O–Ti bond, and the weaker peak at 529.7 eV corresponds to the oxygen in the Ti–O–Ti bond [27,28,39]. This result reveals that C–O–Ti was the dominant structure on TiO_2 surfaces, hinting that ethylene glycol was attached to the TiO_2 surface via the formation of covalent bonds. After organophosphorylation, only one peak of the O 1s was found at 531.2 eV, which was related to the oxygen in the P═O bond and the Ti–O–P bonds. Furthermore, it was noted that the +1.5 eV shift from the Ti-bonded oxygen (529.7 eV) to the P-bonded oxygen (531.2 eV) and −1.3 eV shift from the C-bonded oxygen (532.5 eV) to P-bonded oxygen (531.2 eV) took place after organophosphorylation, which was in good agreement with the results in the literature [27,28,39]. In addition, these changes confirmed the replacement of ethylene glycol by ATMP on the titania surface via the formation of Ti-O-P bonds with Ti atoms.

3.2. Characterizations of CS–OPTi hybrid membranes

The hybrid membranes were prepared using CS as the polymer matrix and OPTi submicrospheres as the fillers via a solution casting method. The cross-section of the resultant membranes was observed by SEM as shown in Fig. 3(a–g). The OPTi fillers were

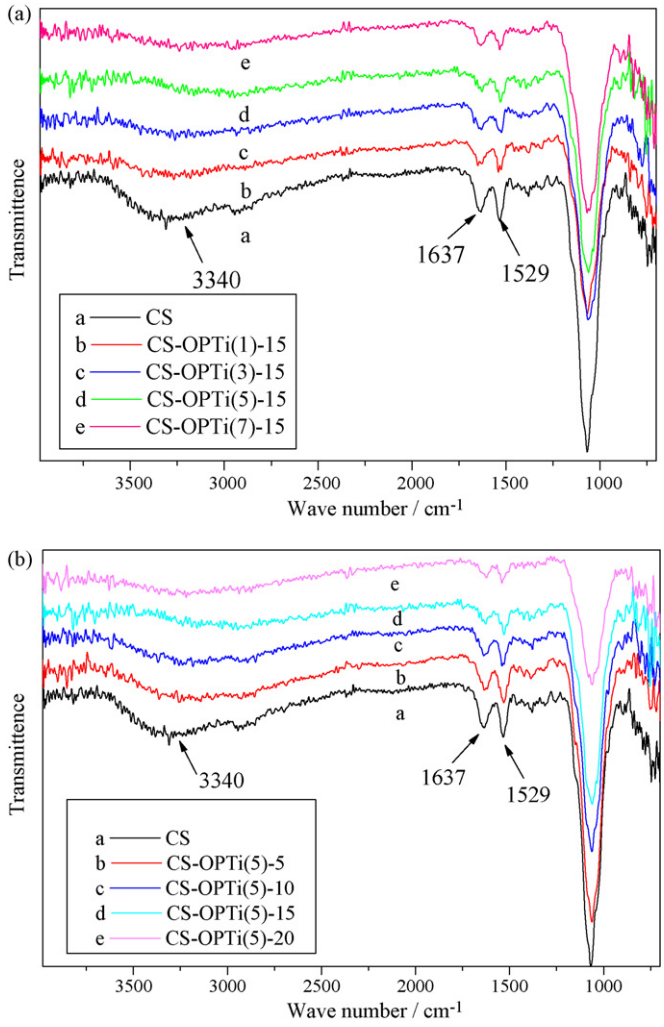

Fig. 4. FTIR spectra of CS and CS–OPTi hybrid membranes with various particle sizes (a) and contents (b).

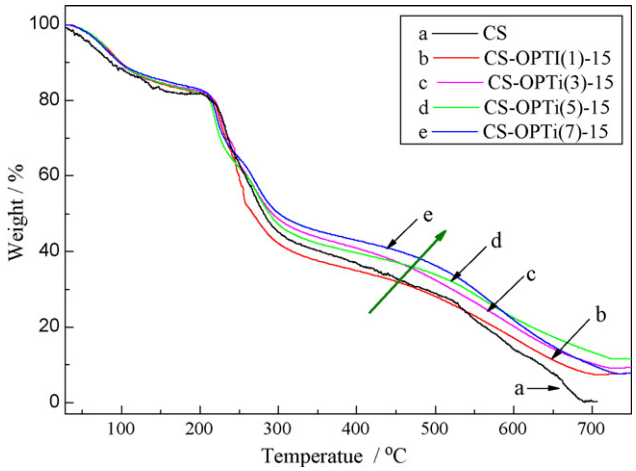

Fig. 5. TGA thermograms of CS and CS–OPTi(*X*)-15 hybrid membranes.

homogenously dispersed in the membrane without sedimentation and obvious agglomeration within the particle size range concerned, and the filler content was deemed below 20% (Fig. 3(g)). This homogeneous dispersion could be attributed to electrostatic repulsion between OPTi particles with phosphonic acid groups on the surface [21] and the strong polymer–filler interfacial interactions.

Fig. 4 shows the FTIR spectra of CS and CS–OPTi membranes. A comparison between the IR spectrum of pure CS membrane and that of CS–OPTi membranes reveals the specific interaction between the polymer and the filler. For the pure CS membrane, the characteristic bands at 3340, 1637 and 1529 cm^{-1} can be attributed to the vibration of hydroxyl, amide I and amide II groups, respectively. After the incorporation of OPTi, strong and rich hydrogen bonds as well as electrostatic attractive forces were generated between the –OH and $–NH_2$ groups on the CS and the $–PO_3H_2$ groups on the OPTi particles, resulting in a remarkable decrease in the intensity of the CS characteristic peaks [12]. This strengthened polymer–filler interaction was found for all four of the OPTi particles types studied, leading to good compatibility in the hybrid membranes, as validated by SEM micrographs. The FTIR spectra of the CS–OPTi(5)-*Y* membranes with various filler contents (Fig. 4(b)) revealed the identical chemical structure. The intensity of the three characteristic peaks for the CS membrane decreased as the OPTi content increased, suggesting an increase of hydrogen bonds and electrostatic attractive force between CS and OPTi.

Thermal stability of the hybrid membrane samples could be inferred from their TGA thermograms in Fig. 5. The CS–OPTi hybrid membranes as well as the CS membrane exhibited similar degradation processes. The first weight loss region (50–100 °C) can be attributed to the evaporation of adsorbed water; the second rapid weight loss around 250 °C is a result of chitosan chain degradation; and the third weight loss region (500–650 °C) corresponds to the degradation of char formed from the chitosan chain degradation [40]. Compared to the pure CS membrane, the presence of OPTi retards the oxidative degradation of CS molecules, leading to an improvement in the membrane thermal stability. The CS–OPTi(1)-15 membrane with the smallest OPTi particles (250 nm) exhibited a slightly poorer thermal stability compared to that of a pure CS membrane, which could be ascribed to the slight aggregation of OPTi particles. The CS–OPTi(7)-15 membrane with the largest OPTi particles (875 nm) exhibited the best thermal stability, which was likely due to the denser polymer chain packing and more pronounced rigidification near the interfacial region. All of the CS–OPTi hybrid membranes showed an onset of degradation at 210 °C, indicating that they were sufficiently stable at desired operating temperatures (<100 °C) for DMFC.

3.3. Water uptake and area swelling degree

Water uptake and the dimensional swelling behavior of membranes both play crucial roles in the determination of methanol permeability and the proton conductivity of proton-exchange membrane fuel cells [31]. Water uptake and the extent of area swelling were measured and plotted in Fig. 6. Compared with the pure CS membrane, both the water uptake and the extent of area swelling of the hybrid membranes decreased with the incorporation of OPTi by approximately 10% (Fig. 6(a)). In addition, both the water uptake and the area swelling of hybrid membranes remarkably decreased with the increase of OPTi content (Fig. 6(b)). Besides the inhibiting effect of the embedded inorganic fillers on the swelling of the polymer matrix, the decrease may also arise due to the less hydrophilic character of the filler. The water uptake of the membranes slightly decrease with the increase of OPTi particle size. The smaller OPTi particles are associated with larger surface energies and are therefore prone to aggregate. Aggregation can encourage the formation of interfacial defects that can play host to more water molecules. The variation in the fractional free volume of the membranes was determined and analyzed by PLAS, as discussed later.

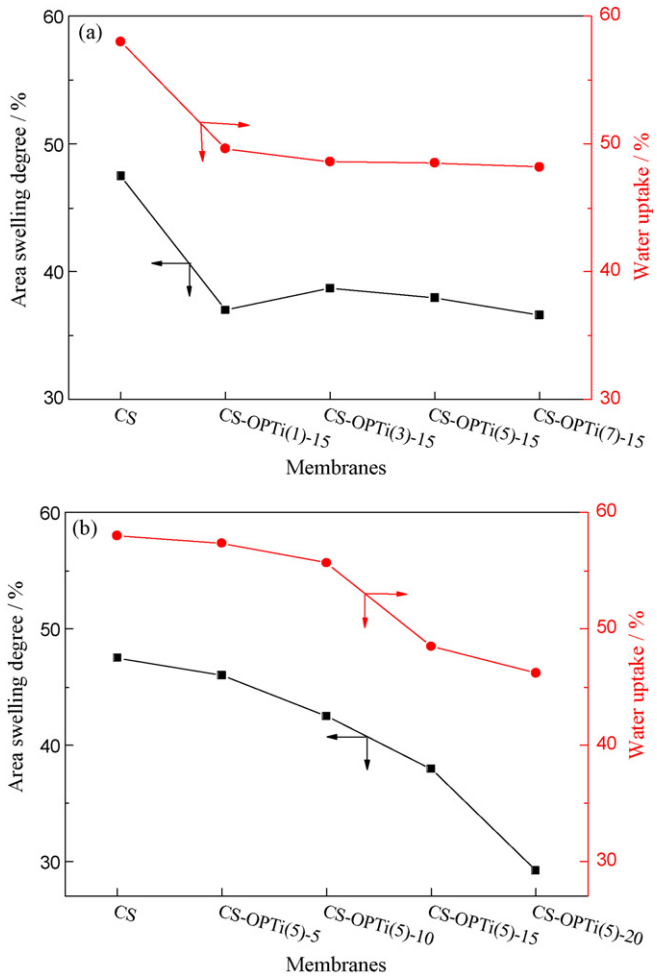

Fig. 6. Area swelling degree and water uptake of CS and CS–OPTi hybrid membranes with various particle sizes (a) and contents (b).

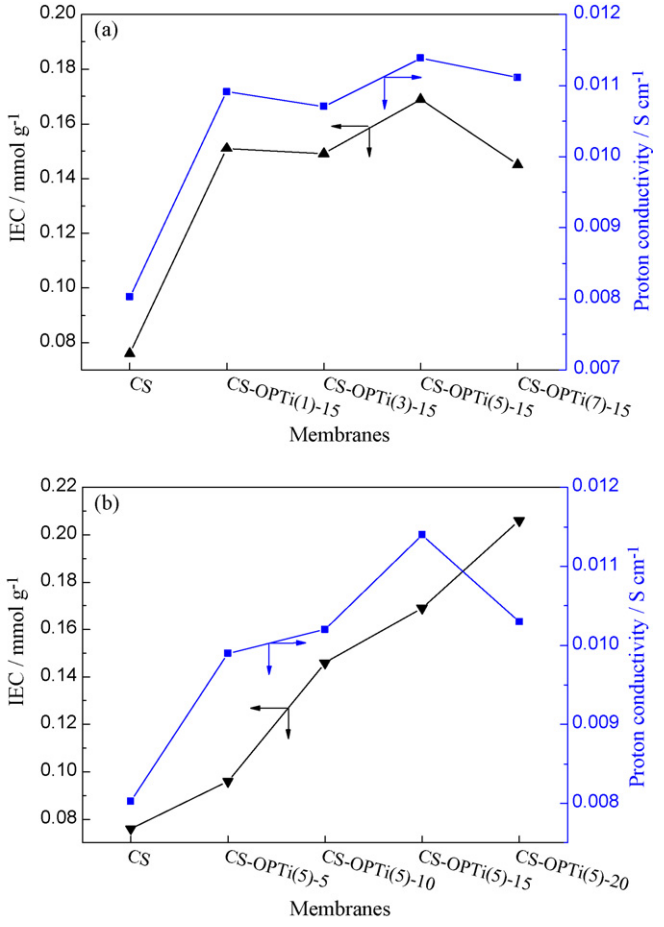

Fig. 7. IEC value and proton conductivity of CS and CS–OPTi hybrid membranes with various particle sizes (a) and contents (b).

3.4. IEC and proton conductivity

Proton conductivity is one of the most important properties of DMFC membranes. Ion-exchange capacity (IEC), an indicator of the density of ionizable hydrophilic functional groups in the membrane, can be used as an indirect but reliable approximation of the proton conductivity. The IEC and proton conductivity for different types of membranes are shown in Fig. 7. It should be added that a proton conductivity of 5.02×10^{-2} S cm^{-1} and an IEC of 0.81 mmol g^{-1} for Nafion® 117 membrane were also acquired for purposed of comparison. The pure CS membrane had the lowest IEC value of 0.076 mmol g^{-1}, due to its poor proton dissociation ability. The IEC values of the hybrid membranes were much higher, due to the presence of $-PO_3H_2$ groups on OPTi. The IEC value of the hybrid membranes varied with the total ATMP content in the membrane, which was consistent with the variation of proton conductivity. The particle size was found to have a slight influence on IEC and proton conductivity (Fig. 7(a)). With an increase in the OPTi content from 5% to 20%, the IEC value increased from 0.096 to 0.206 mmol g^{-1} (Fig. 7(b)). This increment was attributed to the presence of acidic groups ($-PO_3H_2$) on OPTi. Compared to the pure CS membrane, the proton conductivities of the hybrid membranes were found to increase by 23.3–42.5% with the OPTi content increasing from 5% to 15%. When the OPTi content reached 20%, a decrease in proton conductivity was observed, due to the poor dispersion and sedimentation of the OPTi particles.

It is believed that both the vehicle mechanism and the Grotthuss mechanism (illustrated in Scheme 2 contribute to the notable increase in proton conductivity after embedding the OPTi submicrospheres [14,41,42]. The proton transfer facilitated by the additional $-PO_3H_2$ groups on titania fillers can be explained in terms of the following two aspects. On one hand, the –POH groups on the titania surface, together with the hydroxyl and amine groups on CS, were available to form hydrogen bonds with adsorbed water molecules [36], contributing to the formation of continuous hydrophilic regions/pathways [41]. These continuous pathways convey more mobile protons in the form of hydronium ions. On the other hand, the ionic bonds between the $-PO_3H_2$ groups and $-NH_2$ groups reduce the energy barrier for proton transport. The proton could travel along the ionic bonds from one functional group to another [41,42]. Because it has been found that the water uptake of the hybrid membrane is smaller compared with the pristine CS membrane, it is supposed that the Grotthuss mechanism might dominate the proton transfer in the CS–OPTi hybrid membranes. Another point was that although the proton conductivity of the as-fabricated hybrid membranes is lower than that of Nafion® 117, it could still reach an acceptable level of >0.01 S cm^{-1} for serving as a proton-exchange membrane for DMFC applications.

3.5. Free volume characteristics analysis and methanol permeability

The free volume in a membrane refers to static voids created by inefficient chain packing or transient gaps generated by thermally induced chain rearrangement, providing low-resistance

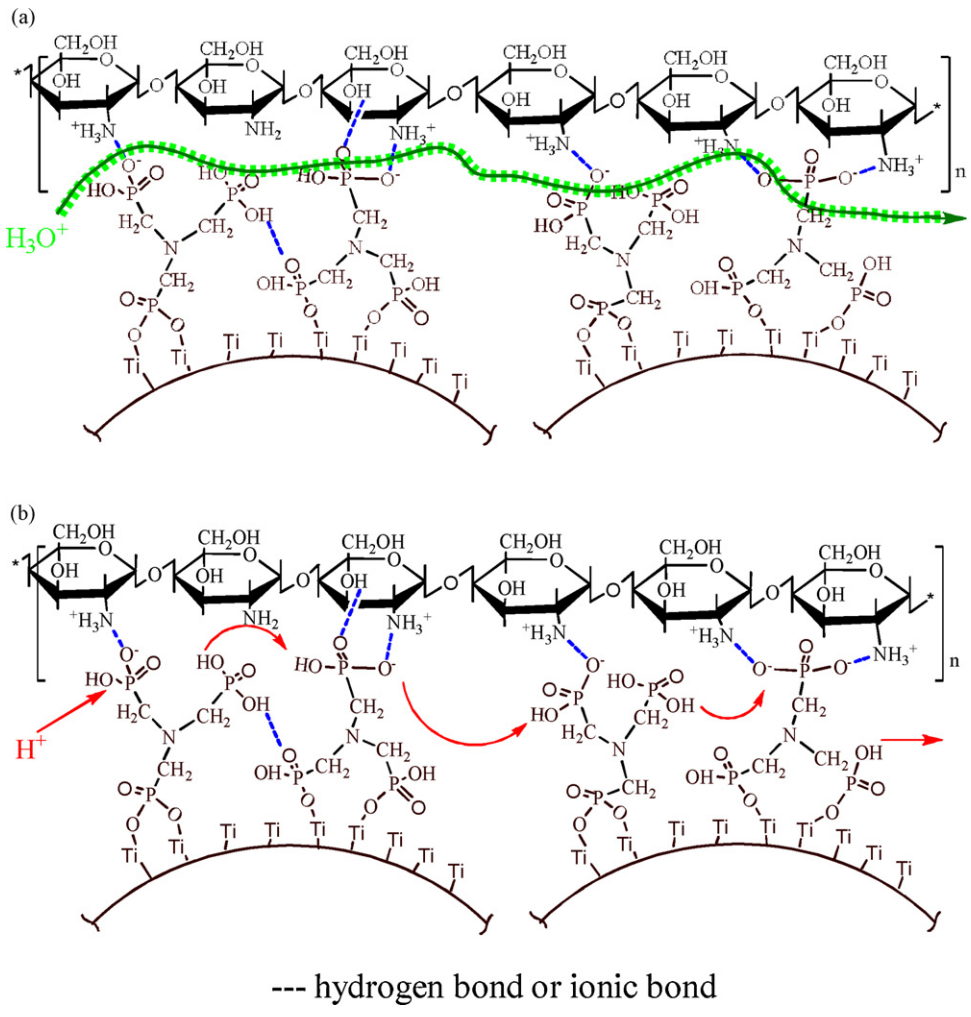

Scheme 2. Proton transfer mechanism in CS–OPTi hybrid membranes: vehicle mechanism (a) and Grotthuss mechanism (b).

paths for molecular transport. The amount of free volume that a dense polymer possesses has a great influence on molecular diffusion. Methanol passes through the DMFC membrane by the solution–diffusion mechanism, wherein the diffusion of methanol is dominant in most cases [7,8]. The larger and more numerous the free volume cavities are, the faster the molecules migrate through the polymer and vice versa.

The influence of inorganic additives on the free volume characteristics of hybrid membranes was investigated by PALS. PALS is a unique and valuable technique which can be exploited for the direct evaluation of the free volume in the membrane. The principle of PALS is based on the free volume module, which assumes that o-Ps is localized in a spherical potential well surrounded by an electron layer with a thickness of Δr equal to 0.1656 nm. The radius of free volume cavity (r) is calculated from pick-off annihilation lifetime (τ) of o-Ps in the free volume elements, and the volume of the equivalent sphere (V_f) and the fractional free volume (*FFV*) are estimated by the following Eqs. [21].

$$\tau = \frac{1}{2}\left[1 - \frac{r}{r+\Delta r} + \left(\frac{1}{2\pi}\right)\sin\left(\frac{2\pi r}{r+\Delta r}\right)\right]^{-1} \quad (6)$$

$$V_f = \frac{4\pi}{3}r^3 \quad (7)$$

$$FFV = V_{f3}I_3 \quad (8)$$

where I is the intensity of o-Ps.

The free volume parameters of the as-prepared membranes are listed in Table 1. The average radius of free volume cavity (r_3) in pure CS membrane was about 0.2883 nm, which is in agreement with the results found in literature [7,21]. In comparison, the addition of OPTi reduced the average radius of free volume cavities and the fractional free volume. It was the strong interaction force between CS and OPTi that inhibited the polymer chain mobility and compressed the polymer chains, cause rigidification near the interfacial region and leading to the free volume shrinkage [21]. As the particle size of OPTi increased, both r_3 and the *FFV* of the hybrid membranes decreased, suggesting compact chain packing at the organic–inorganic interface. The same changing trend was found when the OPTi content increased—both r_3 and *FFV* decreased. Especially for the membrane with 20% OPTi, the *FFV* decreased as much as 11.1%, compared to pure CS membrane.

Table 1
Free volume parameters of CS and CS–OPTi hybrid membranes.

Membranes	τ_3 (ns)	I_3 (%)	r_3 (nm)	V_3 (nm^3)	*FFV* (%)
CS	2.038	16.1	0.2883	0.1004	1.616
CS–OPTi(1)-15	2.042	15.4	0.2887	0.1008	1.552
CS–OPTi(3)-15	2.008	15.6	0.2856	0.0976	1.523
CS–OPTi(5)-15	2.010	15.2	0.2858	0.0978	1.487
CS–OPTi(7)-15	1.988	15.7	0.2837	0.0956	1.501
CS–OPTi(5)-5	2.037	15.9	0.2882	0.1003	1.595
CS–OPTi(5)-10	2.026	16.0	0.2872	0.0992	1.587
CS–OPTi(5)-20	1.999	15.0	0.2839	0.0958	1.437

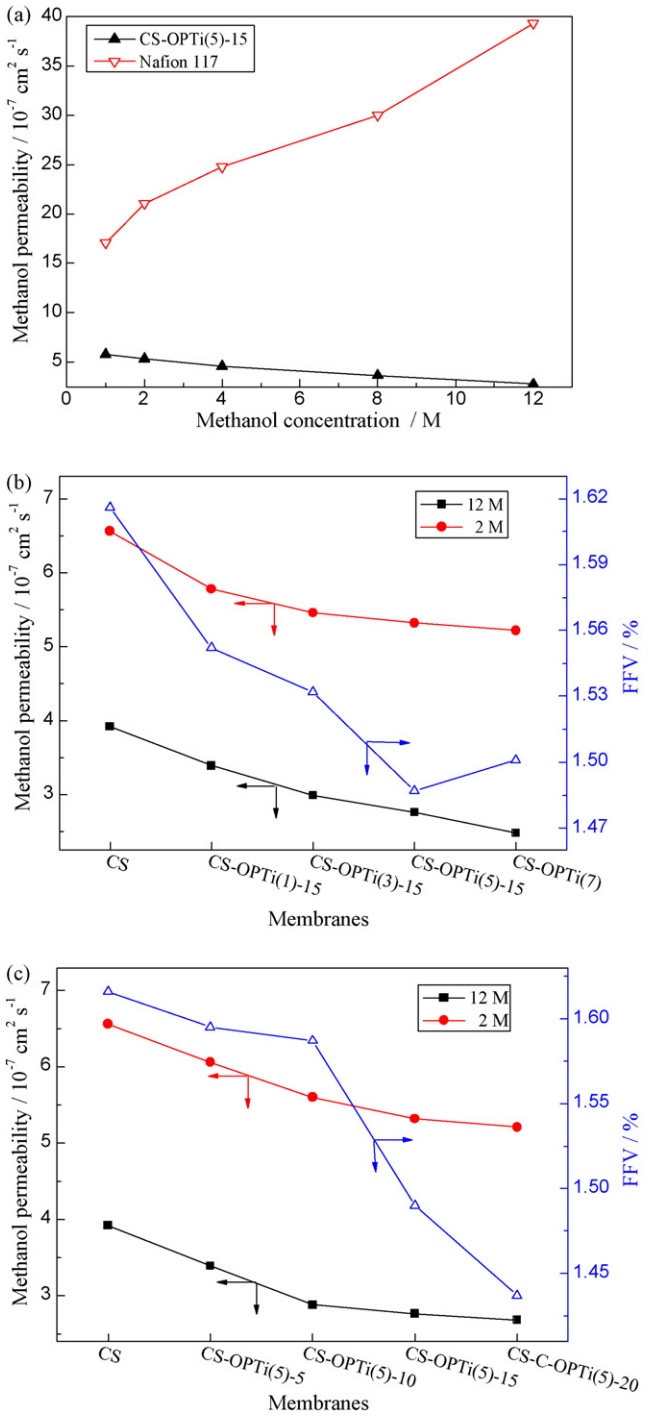

Fig. 8. Methanol permeability of CS–OPTi hybrid membranes versus methanol concentration (a); methanol permeability and *FFV* of CS and CS–OPTi hybrid membranes with various particle sizes (b) and contents (c).

The methanol permeabilities of the CS–OPTi membranes and the Nafion® 117 membrane in methanol solutions of various concentrations are shown in Fig. 8. The methanol permeability of the CS–OPTi(5)-15 membrane was remarkably lower than that of Nafion® 117 under identical methanol concentrations (1–12 M) (Fig. 8(a)). Furthermore, with the increase in methanol concentration, the hybrid membrane exhibited a decrease in methanol permeability while an opposite tendency was found for Nafion® 117. The reduced methanol permeability for hybrid membranes compared with Nafion can be attributed to the inherent alcohol-rejecting property of CS. The methanol resistance property of various CS–OPTi hybrid membranes is shown in Fig. 8(b and c). As the particle size was increased from 250 to 875 nm, the membranes displayed a reduced methanol permeability by 10.4% and 26.8% for 2 and 12 M methanol feeds, respectively. With the increase of OPTi content, the methanol permeability decreased. All of these results arise from the reduced free volume and the twisted pathway for methanol transport after the incorporation of OPTi particles.

4. Conclusions

In this study, organophosphorylated titania submicrospheres with different particle sizes (250–875 nm) were synthesized by an ATMP treatment of titania, and CS–OPTi hybrid membranes were fabricated. The phosphonic acid functionalization of the titania particles enhanced the proton conductivity of the hybrid membrane. The strong interactions between OPTi and CS polymer inhibited the chitosan chain mobility, decreased the membrane free volume fraction and decreased the degree of swelling, thus resulting in reduced methanol permeability. Among all of the as-prepared hybrid membranes, CS–OPTi(5)-15 exhibited a proton conductivity of 11.4 mS cm^{-1} and a methanol permeability of 2.8×10^{-7} cm^2 s^{-1} at a 12 M methanol feed, exhibiting promising potential for practical application in DMFC.

Acknowledgement

The authors gratefully acknowledge support from the National Nature Science Foundation of China (No. 20776101), the Program for Changjiang Scholars and Innovative Research Team in University from the Ministry of Education of China, the Project-sponsored by SRF for ROCS, State Education Ministry and the National Basic Research Program of China (No. 2008CB617502).

References

[1] R.F. Service, Science 296 (2002) 1222–1224.
[2] J. Jagur-Grodzinski, Polym. Adv. Technol. 18 (2007) 785–799.
[3] V. Neburchilov, J. Martin, H.J. Wang, J.J. Zhang, J. Power Sources 169 (2007) 221–238.
[4] S.P. Jiang, Z.G. Liu, Z.Q. Tian, Adv. Mater. 18 (2006) 1068–1072.
[5] T. Sancho, J. Soler, M.P. Pina, J. Power Sources 169 (2007) 92–97.
[6] B. Libby, W.H. Smyrl, E.L. Cussler, AIChE J. 49 (2003) 991–1001.
[7] J.T. Wang, X.H. Zheng, H. Wu, B. Zheng, Z.Y. Jiang, X.P. Hao, B.Y. Wang, J. Power Sources 178 (2008) 9–19.
[8] Z.X. Liang, T.S. Zhao, J. Prabhuram, J. Membr. Sci. 283 (2006) 219–224.
[9] M. Aparicio, J. Mosa, M. Etienne, A. Durán, J. Power Sources 145 (2005) 231–236.
[10] F. Mura, R.F. Silva, A. Pozio, Electrochim. Acta 52 (2007) 5824–5828.
[11] N.H. Jalani, K. Dunn, R. Datta, Electrochim. Acta 51 (2005) 553–560.
[12] Y.L.L. Suryani, J. Membr. Sci. 332 (2009) 121–128.
[13] J. Sauk, J. Byun, H. Kim, J. Power Sources 143 (2005) 136–141.
[14] Z.M. Cui, W. Xing, C.P. Liu, J.H. Liao, H. Zhang, J. Power Sources 188 (2009) 24–29.
[15] C. Yang, S. Srinivasan, A.B. Bocarsly, S. Tulyani, J.B. Benziger, J. Membr. Sci. 237 (2004) 145–161.
[16] F. Bauer, M. Willert-Porada, J. Power Sources 145 (2005) 101–107.
[17] A. Matsuda, T. Kanzaki, K. Tadanaga, M. Tatsumisago, T. Minami, Electrochim. Acta 47 (2001) 939–944.
[18] D.A. Boysen, T. Uda, C.R.I. Chisholm, S.M. Haile, Science 303 (2004) 68–70.
[19] J.C. McKeen, Y.S. Yan, M.E. Davis, Chem. Mater. 20 (2008) 3791–3793.
[20] H. Wu, B. Zheng, X.H. Zheng, J.T. Wang, W.K. Yuan, Z.Y. Jiang, J. Power Sources 173 (2007) 842–852.
[21] J.T. Wang, H. Zhang, Z.Y. Jiang, X. Yang, L.L. Xiao, J. Power Sources 188 (2009) 64–74.
[22] K. Wang, S. McDermid, J. Li, N. Kremliakova, P. Kozak, C.J. Song, Y. Tang, J.L. Zhang, J.J. Zhang, J. Power Sources 184 (2008) 99–103.
[23] Y.G. Jin, S.Z. Qiao, J.C. Diniz da Costa, B.J. Wood, B.P. Ladewig, G.Q. Lu, Adv. Funct. Mater. 17 (2007) 3304–3311.
[24] R. Gosalawit, S. Chirachanchai, S. Shishatskiy, S.P. Nunes, J. Membr. Sci. 323 (2008) 337–346.
[25] S.Z. Ren, G.Q. Sun, C.N. Li, S.Q. Song, Q. Xin, X.F. Yang, J. Power Sources 157 (2006) 724–726.
[26] X.C. Jiang, T. Herricks, Y.N. Xia, Adv. Mater. 15 (2003) 1205–1209.
[27] L. Körösi, S. Papp, I. Bertóti, I. Dékány, Chem. Mater. 19 (2007) 4811–4819.
[28] D. Zhao, C.C. Chen, Y.F. Wang, H.W. Ji, W.H. Ma, L. Zang, J.C. Zhao, J. Phys. Chem. C 112 (2008) 5993–6001.

[29] A. Saccà, A. Carbone, E. Passalacqua, A. D'Epifanio, S. Licoccia, E. Traversa, E. Sala, F. Traini, R. Ornelas, J. Power Sources 152 (2005) 16–21.
[30] B.R. Matos, E.I. Santiago, F.C. Fonseca, M. Linardi, V. Lavayen, R.G. Lacerda, L.O. Ladeira, A.S. Ferlauto, J. Electrochem. Soc. 154 (2007) B1358–B1361.
[31] M. Luisa Di Vona, Z. Ahmed, S. Bellitto, A. Lenci, E. Traversa, S. Licoccia, J. Membr. Sci. 296 (2007) 156–161.
[32] S.J. Paddison, K.D. Kreuer, J. Maier, Phys. Chem. Chem. Phys. 8 (2006) 4530–4542.
[33] W.H.J. Hogarth, J.C. Diniz da Costa, G.Q. (Max) Lu, Solid acid membranes for high temperature (>140 °C) proton exchange membrane fuel cells, J. Power Sources 142 (2005) 223–237.
[34] A.L. Rusanov, P.V. Kostoglodov, M.J.M. Abadie, V.Y. Voytekunas, D.Y. Likhachev, Adv. Polym. Sci. 216 (2008) 125–155.
[35] V.V. Binsu, R.K. Nagarale, V.K. Shahi, J. Mater. Chem. 15 (2005) 4823–4831.
[36] A.G. Kannan, N.R. Choudhury, N.K. Dutta, J. Membr. Sci. 333 (2009) 50–58.
[37] D. Wang, R. Yu, N. Kumada, N. Kinomura, Chem. Mater. 11 (1999) 2008–2012.
[38] T.Y. Ma, X.J. Zhang, G.S. Shao, J.L. Cao, Z.Y. Yuan, J. Phys. Chem. C 112 (2008) 3090–3096.
[39] N.P. Huang, R. Michel, J. Voros, M. Textor, R. Hofer, A. Rossi, D.L. Elbert, J.A. Hubbell, N.D. Spencer, Langmuir 17 (2001) 489–498.
[40] Y.L. Liu, C.Y. Hsu, Y.H. Su, J.Y. Lai, Biomacromolecules 6 (2005) 368–373.
[41] B. Smitha, S. Sridhar, A.A. Khan, Macromolecules 37 (2004) 2233–2239.
[42] J. Ramírez-Salgado, Electrochim. Acta 52 (2007) 3766–3778.